arXiv:1410.5198v1 [cond-mat.str-el] 20 Oct 2014

Phase diagram of exciton condensate in doped two-band Hubbard model

Jan Kuneš[1]

[1]*Institute of Physics, Academy of Sciences of the Czech republic, Cukrovarnická 10, Praha 6, 162 53, Czech Republic**

(Dated: October 21, 2014)

Using the dynamical mean-field approximation we investigate formation of excitonic condensate in the two-band Hubbard model in the vicinity of the spin-state transition. With temperature and band filling as the control parameters we realize all symmetry allowed spin-triplet excitonic phases, some exhibiting a ferromagnetic polarization. While the transitions are first-order at low temperatures, at elevated temperatures continuous transitions are found that give rise to a multi-critical point. Rapid but continuous transition between ferromagnetic and non-magnetic excitonic phases allows switching of uniform magnetization by small changes of chemical potential.

PACS numbers: 71.35.Lk,71.27.+a,05.30.Jp,75.45+j

I. INTRODUCTION

Strongly correlated fermions attract interest for their strong response to various external perturbations. This feature is often connected to existence of competing phases which can be switched by small changes of physical parameters. One way to materials with rich phase diagrams is to look for ordered states characterized by order parameters with complex structure. A prototypical example is superfluidity of ^{3}He where the order parameter is a complex 3×3 matrix, resulting in numerous thermodynamic phases[1]. Common types of order such as charge and spin density waves or s-wave superconductivity usually support only a single phase for a given translational symmetry. Ordered states that allow multiple phases such as p-wave superconductor or excitonic condensate (EC) are more exotic.

The idea of excitonic instability at the semiconductor-semimetal transition was introduced by Mott in 1961[2] and the early developments on the topic were summarized by Halperin and Rice[3,4]. More recently the EC concept was used to study hexaborides[5–8] and bi-layer systems[9–11], where the EC is driven by inter-atomic Coulomb interaction. A possibility of EC driven by intra-atomic Coulomb interaction was proposed recently for $5d^4$ and $3d^6$ perovskites.[12,13]

A minimal model of EC consists of two electronic bands with a small gap/overlap close to half filling and an inter-band Coulomb interaction providing the pairing glue. The theory of EC is formally similar to the theory of superconductivity. However, since the EC order parameter is orbital off-diagonal it may possess both the spin-singlet and spin-triplet components even when being local (s-wave). For weak exchange, typical of inter-atomic interaction, the singlet and triplet excitons are of comparable energy and the order parameter has four complex components[4], allowing numerous thermodynamic phases. In particular, excitonic ferromagnetism may arise from mixing of the singlet and triplet pairing states[14]. Strong ferromagnetic exchange, materialized in intra-atomic Hund's coupling, suppresses the singlet pairing state. While the number of the permissible phases is thus reduced it remains larger than one.

Starting with the early theoretical studies, the weak-coupling approach leading to a BCS-like mean-field theory has been used to describe the EC [5,8,15,16]. The strong-coupling approach was taken by Balents[6]. A special instance of the strong-coupling EC theory is obtained for bi-layer Heisenberg model treated in bond-basis.[17–19] Heavier numerical methods that do not rely on expansions in the interaction strength have only recently been employed. Rademaker *et al.*[10,11] used quantum Monte-Carlo and Kaneko *et al.*[20] used variational cluster approximation to investigate the EC in two-band Hubbard model without the exchange interaction. Kuneš and Augustinský performed a dynamical mean-field calculations on the two-band Hubbard model with strong Hund's exchange and found an excitonic instability close to the spin-state crossover[21]. Subsequently the calculations were extended to study the physics of the ordered phase below the excitonic T_c.[13] The role of Hund's exchange in selecting the singlet and triplet EC order was addressed in variational cluster study by Kaneko and Ohta[22].

The work reported in this Article is a continuation of our effort to map the instabilities occurring in systems close to the spin-state crossover as described by the two-band Hubbard model. Close to the half-filling the physics of the model is governed by the competition between the crystal field and Hund's exchange.[23,24] In the vicinity of the high-spin–low-spin crossover the degeneracy of the corresponding atomic states leads to long-range ordering. For strongly asymmetric bands, the system behaves as the classical Blume-Emery-Griffiths model[25] with high-spin–low-spin order when on bipartite lattice.[26] For less asymmetric bands, the quantum effects gain on importance and the system becomes unstable towards excitonic condensation.[21] Due to its complex nature the excitonic pairing allows several distinct thermodynamic phases. In this work, we map out the EC phase diagram as a function of temperature and band filling. Going beyond the previously studied doping levels we are able to observe all the symmetry allowed phases. In particular, in ad-

dition to the spin-density-wave phase observed close to half-filling[13,22] we observe two ferromagnetic phases.

II. COMPUTATIONAL PROCEDURE

We consider the two-band Hubbard model with nearest-neighbor (nn) hopping on a bipartite (square) lattice with the kinetic $H_{\rm t}$ and the interaction $H_{\rm int} = H^{\rm dd}_{\rm int} + H'_{\rm int}$ terms given by

$$
\begin{aligned}
H_{\rm t} &= \frac{\Delta}{2}\sum_{i,\sigma}\left(n^a_{i\sigma} - n^b_{i\sigma}\right) + \sum_{i,j,\sigma}\left(t_a a^\dagger_{i\sigma}a_{j\sigma} + t_b b^\dagger_{i\sigma}b_{j\sigma}\right) \\
&+ \sum_{\langle ij\rangle,\sigma}\left(V_1 a^\dagger_{i\sigma}b_{j\sigma} + V_2 b^\dagger_{i\sigma}a_{j\sigma} + c.c.\right) \\
H^{\rm dd}_{\rm int} &= U\sum_i\left(n^a_{i\uparrow}n^a_{i\downarrow} + n^b_{i\uparrow}n^b_{i\downarrow}\right) + (U-2J)\sum_{i,\sigma} n^a_{i\sigma}n^b_{i-\sigma} \\
&+ (U-3J)\sum_{i\sigma} n^a_{i\sigma}n^b_{i\sigma} \\
H'_{\rm int} &= J\sum_{i\sigma} a^\dagger_{i\sigma}b^\dagger_{i-\sigma}a_{i-\sigma}b_{i\sigma} + J'\sum_i\left(a^\dagger_{i\uparrow}a^\dagger_{i\downarrow}b_{i\downarrow}b_{i\uparrow} + c.c.\right).
\end{aligned}
\tag{1}
$$

Here $a^\dagger_{i\sigma}$, $b^\dagger_{i\sigma}$ are the creation operators of fermions with spin $\sigma =\uparrow,\downarrow$ and $n^c_{i\sigma} = c^\dagger_{i\sigma}c_{i\sigma}$. The parameters of the Hamiltonian are the same as in Refs. 13,21: U=4, J=1, $\Delta = 3.40$, $V_{1,2} = 0$, $t_a = 0.4118$, and $t_b = -0.1882$. We assume eV to be the unit of energy and express temperature in Kelvin. The choice $t_a t_b < 0$ ensures a ferro EC order[21] allowing us to work with a one-site unit cell.

The numerical calculations were performed in the dynamical mean-field approximation[27,28] with the density-density interaction $H^{\rm dd}_{\rm int}$ only. The effect of adding $H'_{\rm int}$ is considered in Section III F. The auxiliary impurity problem is solved using the hybridization-expansion continuous-time quantum Monte Carlo (CT-HYB)[29,30] in the so called segment implementation, modified to allow off-diagonal hybridization. The spectral functions were obtained with maximum entropy method.[31]

The convergence of the DMFT loop for parameters close to the phase boundaries required several thousands of iterations (typical value far from the boundaries was 20-40 iterations) and was usually checked by starting the iterative procedure in both phases.

III. NUMERICAL RESULTS

In this section we present the DMFT results obtained for the Hamiltonian $H_t + H^{\rm dd}_{\rm int}$. The variable parameters are the temperature T and the hole doping n_h. The excitonic condensate can be characterized by a complex 2-component local order parameter $\phi = (\phi^x, \phi^y)$

$$
\phi^\gamma = \sum_{\alpha\beta}\sigma^\gamma_{\alpha\beta}\langle a^{i\dagger}_\alpha b^i_\beta\rangle, \tag{2}
$$

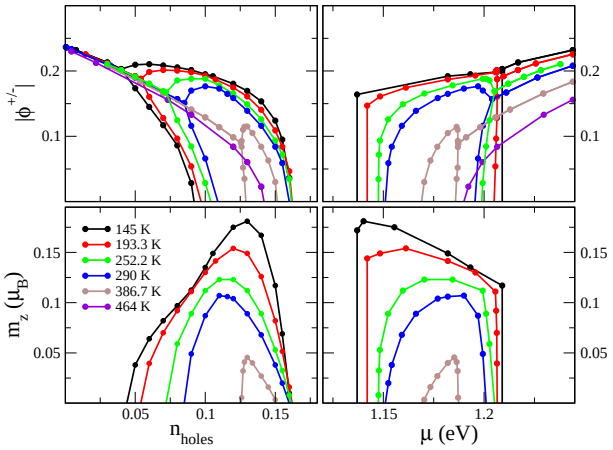

FIG. 1: (color online) Dependence of the order parameters $|\phi^+|$ and $|\phi^-|$ (top row) and the net magnetization (bottom row) on the the doping n_h (left) and chemical potential μ (right) for several temperatures. We point out that n_h-dependences for (n_h, T) falling into the phase separation regime, which correspond to an unphysical (unstable) phase, are not distinguished in the plot.

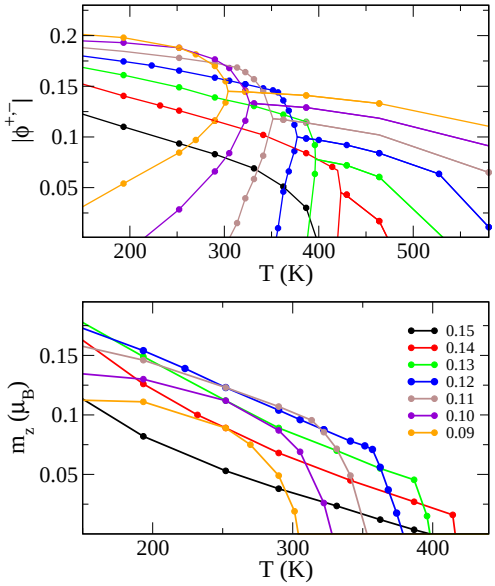

FIG. 2: (color online) The temperature dependence of the order parameters $|\phi^+|$ and $|\phi^-|$ (top) and the net magnetization (bottom) at fixed doping. We point out that results for (n_h, T) falling into the phase separation regime, which correspond to an unphysical (unstable) phase, are not distinguished in the plot.

where σ^γ ($\gamma = x, y$) are the Pauli matrices. Throughout the paper we will use the representation $(\phi^+, \phi^-) = (\phi^x + i\phi^y, \phi^x - i\phi^y)/2$, which is more practical for our purposes. Due to the symmetry of Hamiltonian (1) a variation of the phase of either ϕ^+ or ϕ^- generates degenerate states. Different thermodynamic phases are, therefore, distinguished by the amplitudes $|\phi^+|$ and $|\phi^-|$.

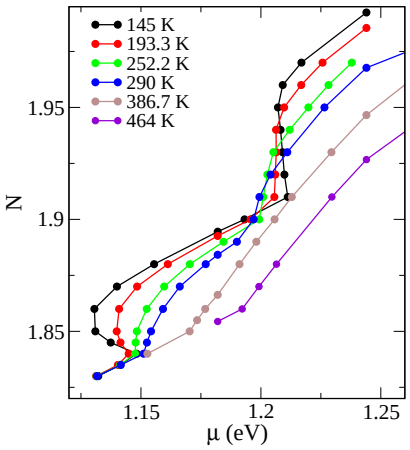

FIG. 3: (color online) The $n(\mu)$ dependence of the charge density on the chemical potential for various temperatures. The line are guides to the eye connecting the points linearly.

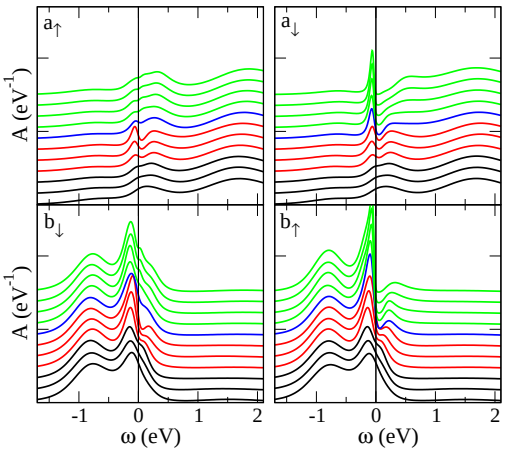

FIG. 4: (color online) The evolution of one-particle spectra with temperature at fixed doping of 0.12 holes/site. The panels show the diagonal spectral functions $A_{\alpha\alpha}(\omega)$ ($\alpha = a_\uparrow$, $a_\downarrow$, $b_\uparrow$, $b_\downarrow$) at various temperatures (offset for clarity). The temperature increases from the top (223.1 K) to the bottom (828.6 K), the colors distinguish the different phases: N (black; 828.6 K, 725 K, 594.9 K), L (red; 527.3 K, 464 K, 386.7 K), E (blue; 362.5 K), and C (green; 341.2 K, 290 K, 252.2 K, 223.1 K).

A. Order parameter and magnetization

In Figs. 1a, 2a we show the evolution of $|\phi^+|$ and $|\phi^-|$ along several constant–n_h and constant–T scans. Four distinct phases can be identified: i) the normal (N) phase $|\phi^+| = |\phi^-| = 0$, ii) the linear (L) excitonic phase $|\phi^+| = |\phi^-| \neq 0$, iii) the circular (C) excitonic phase $|\phi^+| = 0$, $|\phi^-| \neq 0$ and iv) the elliptic (E) excitonic phase $0 \neq |\phi^+| \neq |\phi^-| \neq 0$. For each (n_h, T) pair we found a unique solution. This is, however, not the case for fixed chemical potential μ at low temperatures. In Fig. 3 we show the electron density per atom N as a function of μ. The plot reveals that some solutions obtained at constant n_h are unstable (negative compressibility). Using the Maxwell construction we can identify the charge separation regions and the first-order transition lines. The order parameter as a function of μ is shown in Fig. 2b.

The C and E phases exhibit a finite uniform magnetization $\langle m_z \rangle$ shown in Figs. 1c,d and Fig. 2b. The ordered magnetization exhibits several unusual features. While ϕ follows the square root $(1 - \frac{T}{T_c})^{1/2}$ dependence expected of a mean-field order parameter, $\langle m_z \rangle \sim 1 - \frac{T}{T_c}$ behaves linearly in the vicinity of the C/N boundary (black line in Fig. 2b). Below the L/E boundary the $\langle m_z \rangle$ appears to follow the square root dependence (orange line in Fig. 2b). While these observations based on a few data points are somewhat speculative we present supporting physical arguments in the discussion. Another feature we want to mention is the great sensitivity of $\langle m_z \rangle$ to variations of the chemical potential in the vicinity of the E phase. This property could be used in construction of devices where magnetization is controlled by a gate voltage.

B. Spectral density

In Fig. 4 we show the evolution of the one-particle spectral density as a function of T for fixed doping $n_h = 0.12$. All the four phases are traversed as the temperature is varied. Similar to the behavior of the undoped system, reported in Ref. 21, the appearance of the off-diagonal self-energy in the EC phase causes a dip in the spectral function, a precursor of a gap. In the L phase the doping prevents the chemical potential from being inside the gap. In the C phase, the system approaches a half-metal-like state where the condensed channel ($a_\downarrow$ and $b_\uparrow$ for $|\phi^-| \neq 0$) is gapped and hosts one electron per site[32], while the uncondensed channel ($a_\uparrow$ and $b_\downarrow$) serves as an electron reservoir. Note, nevertheless, that the changes to the $a_\uparrow$ and $b_\downarrow$ spectral densities in the C phase go beyond a simple rigid band shift of the corresponding normal phase spectra. For non-zero cross-hopping $V_{1,2}$ the condensed and uncondensed channels cannot be strictly defined and this picture applies only approximately.

C. Phase diagram

In Fig. 5 we summarize our main result, the phase diagrams in the $n_h - T$ and $\mu - T$ planes. The undoped system undergoes a continuous transition to the L phase where it stays down to the lowest studied temperature (145 K). The instability of the normal phase shifts to lower T_c with doping and excitonic phase disappears completely above 0.17 holes/site. The continuous N/L transition changes into a continuous N/C transition

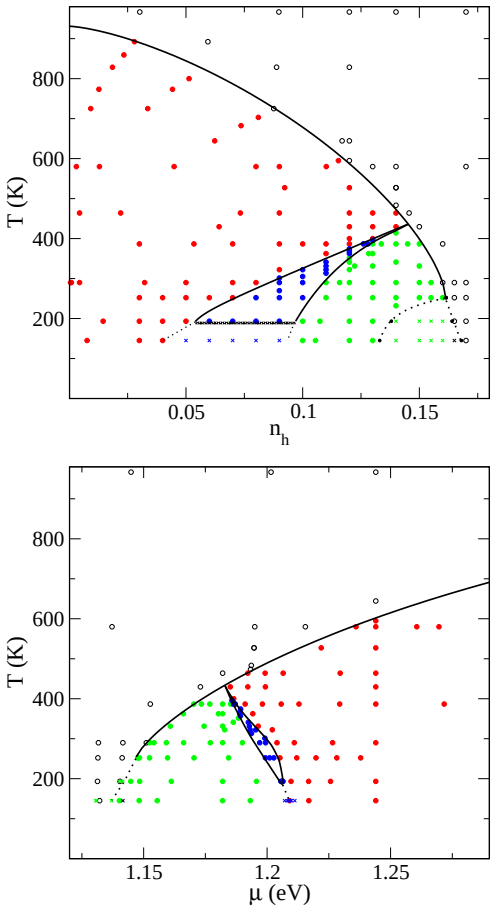

FIG. 5: (color online) Top: the phase diagram in the density-temperature ($n_h - T$) plane. The symbols correspond to the parameters where actual calculations were performed. The circles mark stable solutions while the crosses the thermodynamically unstable ones. The colors code the thermodynamic phases: N (open circles), L (red), E (blue), and C (green) The lines mark the estimated phase boundaries corresponding to continuous transitions (solid) and the phase separation region (dotted). Bottom: the corresponding phase diagram in the $\mu - T$ plane. The solid lines mark the continuous transitions, while the dotted lines the first order ones.

around the doping of 0.145 holes/site. At even higher dopings the N/C transition becomes first-order. The E phase is found in a narrow wedge between the L and C phases. Below approximately 190 K the E phase disappears and the system evolves between L and C phases through a first-order transition.

All four phases appear to come together at a multi-critical point $(n_h, T) \approx$(0.145,430 K). It is not possible for our numerical method to capture details of this region, e.g., to exclude a short but finite E/N boundary. Nevertheless, we present an analysis based on the Landau theory, which supports the phase diagram as drawn in Fig. 5.

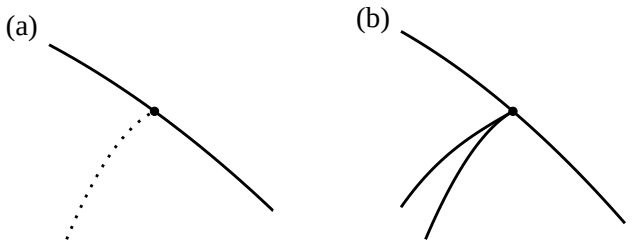

FIG. 6: The two possible shapes of the phase boundaries in the vicinity of the multi-critical point. (a) A first-order transition between C and L phases, (b) two second-order transitions with E phase in between. The second-order transition lines (or the boundaries of the co-existence region) approach the multi critical point with the same slope.

D. Landau functional

The symmetry of our model restricts the form of the Landau functional to

$$F(|\phi^+|, |\phi^-|) = \alpha \left(|\phi^+|^2 + |\phi^-|^2\right) + \beta_0 \left(|\phi^+|^2 + |\phi^-|^2\right)^2 + \beta_1 \left(|\phi^+|^2 - |\phi^-|^2\right)^2 + \ldots, \quad (3)$$

where the higher oder terms contain all powers of $|\phi^+|^2 + |\phi^-|^2$ and even powers of $|\phi^+|^2 - |\phi^-|^2$. The terms up to 4th order in ϕ are sufficient to show that for a finite β_1 a continuous transition to either C phase (for $\beta_1 < 0$ and $\beta_0 > -\beta_1$) or L phase (for $\beta_1 > 0$ and $\beta_0 > 0$) is obtained. The L/N and C/N second-order phase boundaries, therefore, meet at a single point ($\beta_1 = 0$). The critical end point of the C/N boundary corresponds to $\beta_0 = -\beta_1$.

The analysis of the phase diagram in the vicinity of the multi-critical point $\beta_1 = 0$ is more complicated and involves the terms up to order ϕ^8. We postpone the details to the Appendix and here present only the main result. The functional form (3) restricts the behavior in the vicinity of the multi-critical point to two possibilities shown in Fig. 6: i) a first-order transition between the C and L phases, ii) two continuous transitions with an intermediate E phase. Moreover, the C/E and L/E boundaries approach the multi-critical point with the same slope. The terms up to the 8th order decide which of the two scenarios is realized. In our model the numerical data show a clear preference for the scenario (ii).

E. Symmetry considerations

Another way to gain insight into the possible phases of the studied model is to analyze the transformation properties of the order parameter $\boldsymbol{\phi}$ under the symmetries of the Hamiltonian (1). We will also consider the qualitative changes to the phase diagram when external magnetic field or cross-hopping $V_{1,2}$ is added. The Hamiltonian

(1) is invariant under a phase change in any of the four spin-orbit flavors. In addition there is a discrete $\mathbb{Z}_2$ symmetry with respect to a π-spin-rotation (simultaneous in the a and b orbitals) about an arbitrary axis perpendicular to z-axis. Taken together the symmetry group can be written as $\Gamma = U_{c_a}(1) \times U_{c_b}(1) \times \{[U_{s_a}(1) \times U_{s_b}(1)] \rtimes \mathbb{Z}_2\}$, where the first two factors correspond to conservation of charge in the a and b-channels, the latter two $U(1)$ factors correspond to conservation of the z-component of spin in the a and b-channels and form a semi-direct product with the $\mathbb{Z}_2$ group containing the π-spin-rotation, e.g., $\{I, \sigma_x\}$. The order parameter transforms as

$$\begin{aligned} R(\boldsymbol{\varphi}) \begin{pmatrix} \phi^+ \\ \phi^- \end{pmatrix} &= e^{i(\varphi_{c_a} - \varphi_{c_b})} \begin{pmatrix} e^{i(\varphi_{s_a} + \varphi_{s_b})}\phi^+ \\ e^{-i(\varphi_{s_a} + \varphi_{s_b})}\phi^- \end{pmatrix} \\ \sigma_x \begin{pmatrix} \phi^+ \\ \phi^- \end{pmatrix} &= \begin{pmatrix} \phi^- \\ \phi^+ \end{pmatrix} \end{aligned} \tag{4}$$

under the rotations (phase variation) R and the π-spin-rotation about the x-axis.

Distinct phases can be found by inspecting the operations which leave the order parameter $\boldsymbol{\phi}$ invariant. Besides the trivial solution corresponding to the normal phase there are three distinct solutions: (i) $0 \neq \phi^+ \neq \phi^- \neq 0$, implying $\varphi_{c_a} = \varphi_{c_b}$ and $\varphi_{s_a} = -\varphi_{s_b}$, yields the E phase with residual symmetry $U(1) \times U(1)$; (ii) $\phi^- \neq \phi^+ = 0$, implying $\varphi_{c_a} - \varphi_{c_b} - \varphi_{s_a} - \varphi_{s_b} = 0$, yields the C phase with residual symmetry $U(1) \times U(1) \times U(1)$; (iii) $|\phi^+| = |\phi^-| \neq 0$, implying $\varphi_{c_a} = \varphi_{c_b}$ and $\varphi_{s_a} = -\varphi_{s_b}$, yields the L phase with residual symmetry $U(1) \times [U(1) \rtimes \mathbb{Z}_2]$. The $\mathbb{Z}_2$ symmetry of the L phase arises from a π-spin-rotation along the axis parallel to ϕ. While 'direction of ϕ' is not well defined in general as one needs two real vectors to capture the information contained in ϕ, the property $|\phi^+| = |\phi^-|$ of the L phase implies that ϕ can be written as a real vector times a phase factor.

The effects of an external magnetic field along the z-axis and the cross-hopping are easily seen. With non-zero external field the $\mathbb{Z}_2$ factor in Γ disappears and thus the L and E phase are not distinguished anymore. With non-zero cross-hopping the symmetry of the Hamiltonian Γ reduces to $U(1) \times [U(1) \rtimes \mathbb{Z}_2]$ (corresponding to applying a condition $\varphi_{c_a} = \varphi_{c_b}$ and $\varphi_{s_a} = \varphi_{s_b}$). As a result the C and E phases are not distinguished any more.

F. Rotationally invariant interaction

While the presented calculations were performed with density-density interaction $H_{\rm int}^{\rm dd}$ only, real materials usually possess the full spin rotational invariance, which is restored by the first term of $H'_{\rm int}$. It is therefore important to show that including $H'_{\rm int}$ does not lead to qualitatively different results. Considering $H'_{\rm int}$ we have to distinguish the case with ($J' \neq 0$) and without ($J' = 0$) pair-hopping, which breaks the separate conservations of a and b charge. The symmetry of Hamiltonian (1) with $H'_{\rm int}$ is $U(1) \times SU(2)$ in the former case and $U(1) \times U(1) \times SU(2)$ in the latter one. We will consider the latter case and show that it leads to the same phases as the density-density interaction with no cross-hopping.

First, we discuss the Landau functional. Treating $\boldsymbol{\phi}$ as a 3-dimensional complex vector the Landau functional must be a rotationally invariant function of two vectors $F(\bar{\boldsymbol{\phi}}, \boldsymbol{\phi})$, which implies that its Taylor expansion must be a polynomial in $\bar{\boldsymbol{\phi}} \cdot \bar{\boldsymbol{\phi}}$, $\boldsymbol{\phi} \cdot \boldsymbol{\phi}$ and $\bar{\boldsymbol{\phi}} \cdot \boldsymbol{\phi}$.[33] Moreover, $F(\bar{\boldsymbol{\phi}}, \boldsymbol{\phi})$ must be invariant with respect to the overall phase of $\boldsymbol{\phi}$ (due to $V_{1,2} = 0$ and $J' = 0$). This reduces the expansion of $F(\bar{\boldsymbol{\phi}}, \boldsymbol{\phi})$ to a polynomial in $\bar{\boldsymbol{\phi}} \cdot \boldsymbol{\phi}$ and $|\bar{\boldsymbol{\phi}} \wedge \boldsymbol{\phi}|^2$. With the z-axis parallel to $i(\bar{\boldsymbol{\phi}} \wedge \boldsymbol{\phi})$ (or any normal to $\boldsymbol{\phi}$ in case the wedge product is zero) the two terms yield the $|\phi^+|^2 + |\phi^-|^2$ and $(|\phi^+|^2 - |\phi^-|^2)^2$ and the equivalence to (3) becomes explicit.

Using the same choice of the coordinates we can repeat the discussion from the previous section. For $|\phi^+| \neq |\phi^-|$ only rotations about the z-axis can preserve $\boldsymbol{\phi}$ and thus we can use expression (4). However, since the spin-flip term does not allow independent spin rotations about the z-axis we have to assume $\varphi_{s_a} = \varphi_{s_b} \equiv \varphi_s$ from the beginning. The symmetries of the E phase thus must fulfill $\varphi_s = 0$ and $\varphi_{c_a} = \varphi_{c_b}$, i.e., only $U(1)$ symmetry corresponding to the conservation of total charge is preserved. The invariance of $\boldsymbol{\phi}$ in the C phase is less restrictive. The condition $\varphi_{c_a} - \varphi_{c_b} - \varphi_s = 0$ leads to residual symmetry $U(1) \times U(1)$ allowing also spin rotations accompanied by change of the relative phase of the a and b orbitals. As in the density-density case, non-zero cross-hopping or pair-hopping removes the distinction between the C and E phases. Finally, if $\bar{\boldsymbol{\phi}} \wedge \boldsymbol{\phi} = 0$ we can choose the z-axis parallel to $\bar{\boldsymbol{\phi}} + \boldsymbol{\phi}$, in which case the only non-zero component of $\boldsymbol{\phi}$, $\phi_z \sim a^\dagger_\uparrow b_\uparrow - a^\dagger_\downarrow b_\downarrow$, is invariant under $U(1) \times U(1)$ corresponding to $z - axis$ spin rotation (besides the overall phase change), which correspond to the $\mathbb{Z}_2$ symmetry of the L phase in the density-density case. Note, that the non-trivial $U(1)$ symmetries of the C and L phase are different. While the former one contains spin-rotations about an axis perpendicular to $\boldsymbol{\phi}$ combined with orbital phase transformations, the latter one consists of pure spin-rotations about an axis 'parallel' to $\boldsymbol{\phi}$.

While the same excitonic phases exist in the model with and without $H'_{\rm int}$ the space of low-energy fluctuations of the order parameter, which reflects the broken symmetries, will be quite different in the two cases. Since our numerical method does not treat these fluctuations we do not discuss them here.

IV. DISCUSSION

The above numerical results have demonstrated the rich phase diagram of the excitonic condensate. The key feature allowing the various phases is the orbital-off-diagonal character, which renders the order parameter complex. Were the order parameter real, such as the

usual spontaneous magnetization, only one phase would have been possible since all real magnetization vectors of the same magnitude can be connected by some spin rotation (This does exclude multiple phases with different translational symmetry, e.g., ferro and antiferro). This is not true for complex vectors. To see this, one can consider the vector product $\bar{\boldsymbol{\phi}} \wedge \boldsymbol{\phi}$, which is invariant under rotations as well as overall phase transformation. Two states characterized by order parameters with the same magnitude $|\boldsymbol{\phi}|^2$ but different $\bar{\boldsymbol{\phi}} \wedge \boldsymbol{\phi}$ cannot be transformed into one another by a symmetry operation of the Hamiltonian. It is easy to see that the L phase corresponds to $\bar{\boldsymbol{\phi}} \wedge \boldsymbol{\phi} = 0$, while for the C phase $|\bar{\boldsymbol{\phi}} \wedge \boldsymbol{\phi}| = |\boldsymbol{\phi}|^2$.

How do the different EC states look like in the direct space? Halperin and Rice[4] have shown that exciton condensation in the spin-triplet channel gives rise either to a spin-density or a spin-current-density wave. Assuming real Wannier orbitals $\psi_a(\mathbf{r})$ and $\psi_b(\mathbf{r})$, and neglecting (although this is not essential) the overlap density of orbitals on different sites, the exciton condensation gives rise to the spin-density $S^\alpha(\mathbf{r})$ and the spin-current density $J^{\alpha\beta}(\mathbf{r})$[6]

$$\begin{aligned} S^\alpha(\mathbf{r}) &= 2\psi_a(\mathbf{r})\psi_b(\mathbf{r})\,\mathrm{Re}\,\phi^\alpha \\ J^{\alpha\beta}(\mathbf{r}) &= (\psi_a(\mathbf{r})\partial_\beta\psi_b(\mathbf{r}) - \psi_a(\mathbf{r})\partial_\beta\psi_b(\mathbf{r}))\,\mathrm{Im}\,\phi^\alpha. \end{aligned} \tag{5}$$

on each lattice site. In our model with $H_{\mathrm{int}}^{\mathrm{dd}}$ only, the spin polarization is confined to x–y plane. Note that the total integrated spin moment or integrated spin current in (5) are zero. Real ϕ thus gives rise to magnetic multipoles, precise form of which depends on the shapes of orbital $\psi_a(\mathbf{r})$ and $\psi_b(\mathbf{r})$. However, since the low lying excitations in general do not correspond to direct space rotations of these multipoles, we do not find it useful to speak about multipole order. In fact, in the present case with $V_{1,2} = 0$ a spin-density state can be continuously 'rotated' into a spin-current state, by varying the phase of $\boldsymbol{\phi}$, without any energy cost. In the L phase, all Cartesian components of $\boldsymbol{\phi}$ can be made simultaneously real or imaginary, thus corresponding to a purely spin-density or a spin-current state. Non-zero cross hopping $V_{1,2}$ removes the degeneracy of spin-density and spin-current states.[5,21]

In the C and E phases, on the other hand, a finite phase difference between the Cartesian components of $\boldsymbol{\phi}$ implies that both the spin density and spin current must be simultaneously present. In these phases, breaking of the $\mathbb{Z}_2$ symmetry in the Hamiltonian with $H_{\mathrm{int}}^{\mathrm{dd}}$ only gives rise to a net spin moment along the z-axis. In case with $SU(2)$ symmetry of the Coulomb interaction, $\boldsymbol{\phi}$ can point in arbitrary direction and the net spin moment is parallel to $i\bar{\boldsymbol{\phi}} \wedge \boldsymbol{\phi}$. As discussed in detail by Balents[5] this ferromagnetic phase is distinct from the excitonic ferromagnetism proposed by Volkov *et al.*[14] which arises from mixing of spin-singlet and spin-triplet orders. Such mixing is possible only for small exchange J.

The present ferromagnetic order is induced by the exciton condensation in the sense that the normal phase

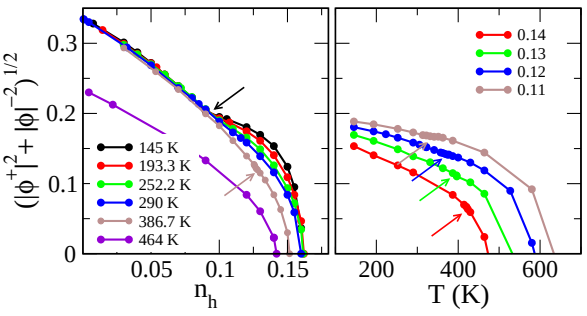

FIG. 7: The magnitude of the order parameter $\sqrt{|\phi^+|^2 + |\phi^-|^2}$. Along the same constant T (right) and constant n_h (left) scans as in Figs. 1 and 2. The arrows mark the narrow region of the E phase.

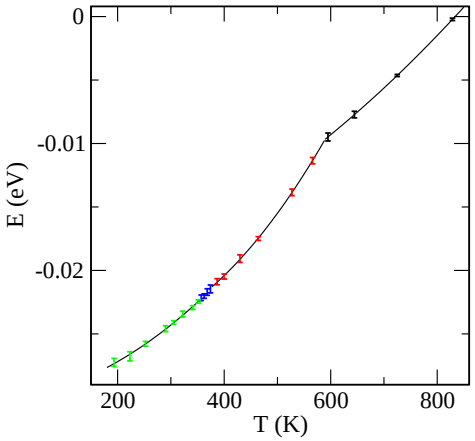

FIG. 8: The internal energy per site as a function of temperature along the $n_h = 0.12$ scan through the phase diagram. The colors of the error bars code the phases as in Fig. 5. The lines represent quadratic fits to the N, L and C phases.

is not close to a ferromagnetic instability. The magnitude of the ordered moment is very small compared to the transition temperature, given there is no geometric frustration in the system. The magnetization close to the N/C boundary follows a linear $1 - \frac{T}{T_c}$ dependence rather than the square root $(1 - \frac{T}{T_c})^{1/2}$ behavior expected of the mean-field order parameter, obeyed by ϕ^-. This behavior is easily understood in both weak and strong coupling mean-field theories which give $\langle m_z \rangle \sim |\phi^-|^2$ in the leading order of the perturbation theory in ϕ^-.

The fundamental nature of $\boldsymbol{\phi}$ as an order parameter can be also seen in Fig. 7 where we plot the magnitude $|\boldsymbol{\phi}|^2$. Both the constant–n_h and constant–T scans show that the L–E–C transition can be viewed as a rotation of the vector $(|\phi^+|, |\phi^-|)$. This is particularly so in the vicinity of the multi-critical point. This observation shows that our numerical data are consistent with the Landau theory and that at the multi-critical point the system has higher symmetry than the Hamiltonian (1).

What determines the stability of the different phases

on the microscopic level? Close to the multi-critical point one can expect separation of energy scales responsible for the condensation itself and for selecting of a particular phase. This separation is clearly visible in Fig. 8 where the internal energy across all the phases is shown along a constant–$n_h = 0.12$ scan. While there is a distinct kink at 790 K where the exciton condensation takes place, the L/E and E/C transitions are hardly discernible within our numerical accuracy.

It is not possible to link the different excitonic phases to particular terms in Hamiltonian (1) in general. It is, nevertheless, instructive to discuss the strong and the weak coupling limits even though, given we are dealing with doped systems, they may provide only a qualitative insight. The strong-coupling Hamiltonian of Ref. 21

$$H_{\text{eff}}^{\text{dd}} = \sum_i \mu n_i + K_\perp \sum_{ij,s} d_{i,s}^\dagger d_{j,s} + \sum_{\langle ij\rangle} \left(K_\parallel n_i n_j + K_0 S_i^z S_j^z\right) + K_1 \sum_{\langle ij\rangle,s} \left(d_{i,s}^\dagger d_{j,-s}^\dagger + d_{i,s} d_{j,-s}\right) \tag{6}$$

describes two flavors $s = \pm 1$ of bosons with the hard-core constraint $n_i = \sum_s d_{i,s}^\dagger d_{i,s} \leq 1$, corresponding to HS states created by $d_1^\dagger = a_\uparrow^\dagger b_\downarrow$ and $d_{-1}^\dagger = a_\downarrow^\dagger b_\uparrow$ out of the LS vacuum. Responsible for condensation of the excitons is the hopping term proportional to $K_\perp$. This term, however, has a higher symmetry than Hamiltonian (1) and does not distinguish between excitonic phases. The stable phase is therefore selected by the K_0 and K_1 terms. If negative the spin exchange term K_0 favors the ferromagnetic C phase, while positive[34] K_0 favors the unpolarized L phase. The K_1 term, present only for $V_{1,2} \neq 0$, yields zero contribution to $\langle d_{i,s}\rangle\langle d_{j,-s}\rangle$ in the C phase, while in the L phase this contribution can be made negative by proper choice of the phase of $\langle d_{i,s}\rangle$. The K_1 term thus favors the L phase. Strong coupling analysis of the case $J \ll K_0, K_\perp$, which requires inclustion of the spin-singlet bosons, can be found in Ref. 5.

In the weak coupling limit the excitonic condensation is driven by the $(U-2J)n_{i\sigma}^a n_{i-\sigma}^b$ term in (1). The repulsion between electrons in the same orbital $U n_{i\uparrow}^a n_{i\downarrow}^a$ favors the polarized C phase over L phase since the expectation value $\langle n_{i\uparrow}^a n_{i\downarrow}^a\rangle$ vanishes in the former.

We close the discussion by a technical remark. While the exciton condensation is obtained also in a static Hartree theory, the full treatment of the local dynamics is crucial to obtain the different excitonic phases. Our brief experimenting with Hartree theory revealed a strong bias towards the polarized C phase, which can be traced back to the minimization of $\langle n_{i\uparrow}^a n_{i\downarrow}^a\rangle$. In a static theory this is achieved by polarizing the system while in the dynamic theory these terms are strongly suppressed already in the normal phase.

V. CONCLUSIONS

Using dynamical mean-field theory we have investigated phase diagram of two-band Hubbard model with strong Hund's coupling in the regime of excitonic instability. The spin-triplet orbital-off-diagonal order parameter allows several thermodynamic phases. Varying temperature and the chemical potential of the system we have observed all the symmetry allowed phases including those with induced ferromagnetic polarization. The transitions at low temperatures are of the first order accompanied by a charge separation. At intermediate temperatures, however, the transitions become continuous. The ferromagnetic polarization exhibits a large reversible response to small changes of the chemical potential in this regime. This effect can be used to construct devices where magnetization is switched reversibly by means of a gate voltage.

Acknowledgments

We thank P. Augustinský, A. Kauch, V. Pokorný, D. Vollhardt, and A. P. Kampf for discussions and valuable suggestions. We acknowledge the support of Deutsche Forschungsgemeinschaft through FOR1346 and the Grant Agency of the Czech Republic through project 13-25251S.

Appendix A

In order to analyze the behavior of (3) in the vicinity of the multi-critical point we write the functional to the 8th order in ϕ and use polar coordinates in the $|\phi^+|$–$|\phi^-|$ plane:

$$\begin{gathered} F(\eta,t) = \alpha\eta + \beta_0\eta^2 + \gamma_0\eta^3 + \delta_0\eta^4 + \\ \left(\beta_1\eta^2 + \gamma_1\eta^3 + \delta_1\eta^4\right) C(t)^2 + \delta_2\eta^4 C(t)^4 \\ |\phi^+| = \eta^{\frac{1}{2}}\cos(t), \quad |\phi^-| = \eta^{\frac{1}{2}}\sin(t), \end{gathered} \tag{A1}$$

where $C(t) = \cos(2t)$. For sufficiently small α and β_1, $F(\eta,t)$ has approximately the form of a Mexican hat with the radial minima $\tilde\eta(t)$ on a circle $\tilde\eta(t) = -\frac{\alpha}{2\beta_0}$. The terms containing $C(t)$ cause a deformation of $\tilde\eta(t)$ from the circular shape and lift the degeneracy of F along $\tilde\eta(t)$. Our strategy will be to analyze this effect in different orders of α. Behavior of the stationary points of $F(\eta,t)$ depends on the direction in which the limit $\beta_1 \to 0, \alpha \to 0^-$ is taken. We specify the limit by introducing a parameter Λ: $\beta_1 = \Lambda\alpha$.

The variation of Landau functional along the contour of radial minima $\tilde\eta(t)$ is given by $\tilde F(t) \equiv F(\tilde\eta(t),t)$. The $\tilde\eta(t)$ itself fulfills the equation

$$\partial_\eta F(\tilde\eta(t),t) = 0. \tag{A2}$$

Solving (A2) in the form of a power series $\tilde{\eta}(t) = K(t)\alpha + L(t)\alpha^2 + M(t)\alpha^3$ we get

$$\begin{aligned} K(t) &= -\frac{1}{2\beta_0} \\ L(t) &= \frac{1}{8\beta_0^3}\left(-3\gamma_0 + 4\Lambda\beta_0 C(t)^2 - 3\gamma_1 C(t)^2\right) \\ M(t) &= \frac{1}{16\beta_0^5}\left(-9\gamma_0 + 4\beta_0\delta_0 + 18\Lambda\beta_0\gamma_0 C(t)^2 18\gamma_0\gamma_1 C(t)^2 + \right. \\ &\quad \left. + 4\beta_0\delta_1 C(t)^2 - 4\Lambda^2\beta_0^2 C(t)^4 - 9\gamma_1^2 C(t)^4 + 4\beta_0\delta_2 C(t)^4\right) \end{aligned} \tag{A3}$$

Substituting this expansion into (A1) we arrive at the expansion of $\tilde{F}(t)$

$$\begin{aligned} \tilde{F}(t) = &\frac{2\Lambda\beta_0 - \gamma_1}{8\beta_0^3}\alpha^3 C(t)^2 \\ &+ \frac{2\beta_0\left(6\Lambda\gamma_0 + \delta_1\right) - 9\gamma_0\gamma_1}{32\beta_0^5}\alpha^4 C(t)^2 \\ &- \frac{16\Lambda^2\beta_0^2 + 9\gamma_1^2 - 4\beta_0\left(6\Lambda\gamma_1 + \delta_2\right)}{64\beta_0^5}\alpha^4 C(t)^4 + o(\alpha^5), \end{aligned} \tag{A4}$$

where we have dropped the t-constant terms. For a general Λ, $C(t)^2$ appears in the order α^3 while $C(t)^4$ appears first in the order α^4. Therefore, with the exception of $\Lambda = \frac{\gamma_0}{2\beta_0}$ where the α^3 term in (A4) vanishes, the $C(t)^2$ term is dominant for a sufficiently small α. $C(t)^2$ has a unique minimum either at $t = 0$ or at $t = \pi/4$, depending on the sign of the prefactor. The functional (A1) in this limit thus yields a single stable phase - the C phase ($t = 0$) for $2\Lambda\beta_0 - \gamma_1 < 0$ and L phase for $2\Lambda\beta_0 - \gamma_1 > 0$. Varying Λ across the $\Lambda = \frac{\gamma_0}{2\beta_0}$ the minimum and maximum of $\tilde{F}(t)$ switch and there is a transition between the C and L phases.

This transition can happen in one of two distinct ways, see Fig. 6. To see this we keep α fixed (and sufficiently small so that all $o(\alpha^5)$ terms in $\tilde{F}(t)$ are irrelevant). In a narrow interval of Λ (of the width of order α) in the vicinity of $\Lambda = \frac{\gamma_0}{2\beta_0}$ the α^3 contribution to $\tilde{F}(t)$ vanishes and $\tilde{F}(t)$ has the form $aC(t)^2 + bC(t)^4$ with coefficients a and b of comparable sizes. This angular form offers only three possibilities for its stationary points: i) the only stationary points are at $t = 0$ and $\pi/4$, in which case one of them must be maximum and the other one minimum corresponding to a single stable phase, either L or C, ii) there is a single local maximum between 0 and $\pi/4$, in which case there must be local minima at 0 and $\pi/4$ corresponding to L and C phases being simultaneously stable, iii) there is a single local minimum between 0 and $\pi/4$ corresponding to the E phase, in which case there must be local maxima at 0 and $\pi/4$ and thus E being the only stable phase. While (i) includes the case where the $C(t)^2$ term is dominant, the transition between the C and L can only take place by passing through (ii), i.e., a first order transition, or (iii), i.e., two continuous transitions with an intermediate E phase.

* Electronic address: kunes@fzu.cz

1 D. Vollhardt and P. Wölfle, *The Superfluid Phases of Helium 3* (Dover Publications, Reprint edition, 2013).
2 N. Mott, Philos. Mag. **6**, 287 (1961).
3 B. I. Halperin and T. M. Rice, Rev. Mod. Phys. **40**, 755 (1968).
4 B. Halperin and T. M. Rice, Solid State Physics **21**, 115 (1968).
5 L. Balents and C. M. Varma, Phys. Rev. Lett. **84**, 1264 (2000).
6 L. Balents, Phys. Rev. B **62**, 2346 (2000).
7 V. Barzykin and L. P. Gor'kov, Phys. Rev. Lett. **84**, 2207 (2000).
8 M. Y. Veillette and L. Balents, Phys. Rev. B **65**, 014428 (2001).
9 J. Eisenstein and A. H. MacDonald, Nature **432**, 691 (2004).
10 L. Rademaker, J. van den Brink, J. Zaanen, and H. Hilgenkamp, Phys. Rev. B **88**, 235127 (2013).
11 L. Rademaker, S. Johnston, J. Zaanen, and J. van den Brink, Phys. Rev. B **88**, 235115 (2013).
12 G. Khaliullin, Phys. Rev. Lett. **111**, 197201 (2013).
13 J. Kuneš and P. Augustinský, arXiv:1405.1191.
14 B. A. Volkov, Y. V. Kopaev, and A. I. Rusinov, JETP **41**, 952 (1975).
15 J. des Cloizeaux, J. Phys. Chem. Solids **26**, 259 (1965).
16 B. Zocher, C. Timm, and P. M. R. Brydon, Phys. Rev. B **84**, 144425 (2011).
17 S. Sachdev and R. N. Bhatt, Phys. Rev. B **41**, 9323 (1990).
18 T. Sommer, M. Vojta, and K. W. Becker, Eur. Phys. J. B **23**, 329 (2001).
19 T. Giamarchi, C. Rüegg, and O. Tchernyschyov, Nat. Phys. **4**, 198 (2008).
20 T. Kaneko, K. Seki, and Y. Ohta, Phys. Rev. B **85**, 165135 (2012).
21 J. Kuneš and P. Augustinský, Phys. Rev. B **89**, 115134 (2014).
22 T. Kaneko and Y. Ohta, arXiv:1407.4872.
23 P. Werner and A. J. Millis, Phys. Rev. Lett. **99**, 126405 (2007).
24 R. Suzuki, T. Watanabe, and S. Ishihara, Phys. Rev. B **80**, 054410 (2009).
25 M. Blume, V. J. Emery, and R. B. Griffiths, Phys. Rev. A **4**, 1071 (1971).
26 J. Kuneš and V. Křápek, Phys. Rev. Lett. **106**, 256401 (2011).
27 A. Georges, G. Kotliar, W. Krauth, and M. J. Rozenberg, Rev. Mod. Phys. **68**, 13 (1996).
28 W. Metzner and D. Vollhardt, Phys. Rev. Lett. **62**, 324 (1989).
29 P. Werner, A. Comanac, L. de' Medici, M. Troyer, and A. J. Millis, Phys. Rev. Lett. **97**, 076405 (2006).
30 E. Gull, A. J. Millis, A. I. Lichtenstein, A. N. Rubtsov, M. Troyer, and P. Werner, Rev. Mod. Phys. **83**, 349 (2011).

[31] J. E. Gubernatis, M. Jarrell, R. N. Silver, and D. S. Sivia, Phys. Rev. B **44**, 6011 (1991).

[32] The numerical value at the lowest studied temperature of 145 K is 0.987.

[33] $\boldsymbol{\phi} \cdot \boldsymbol{\phi} = \phi_x \phi_x + \phi_y \phi_y + \phi_z \phi_z$.

[34] The actual strong coupling expression gives always positive K_0.